
This manuscript is a preprint and has been submitted for publication in **Petroleum Geoscience**. This manuscript has not undergone peer-review. Subsequent versions of this manuscript may have different content. If accepted, the final version of this manuscript will be available via the '*Peer-reviewed Publication DOI*' link on the right-hand side of this webpage.

Please feel free to contact the authors directly. Feedback is welcome.

The competition for salt and kinematic interactions between minibasins during density-driven subsidence: observations from numerical models.

Naiara Fernandez^{a*}, Michael R. Hudec^a, Christopher A-L Jackson^b, Tim P. Dooley^a, Oliver B. Duffy^a

^a*Bureau of Economic Geology, Jackson School of Geosciences, The University of Texas at Austin, University Station, Box X, Austin, Texas, 78713-8924, USA*

^b*Basins Research Group (BRG), Department of Earth Science & Engineering, Imperial College, Prince Consort Road, London, United Kingdom, SW7 2BP, UK*

*Corresponding author: naiara.fernandez@beg.utexas.edu

Abstract

Stratal geometries of salt-floored minibasins provide a record of the interplay between minibasin subsidence and sedimentation. Minibasin subsidence and resulting stratal geometries are frequently interpreted by considering the minibasins in isolation and implicitly assuming that internal geometries are the result of purely vertical halokinetic processes. However, minibasins rarely form in isolation and may record complex subsidence histories even in the absence of lateral tectonic forces. In this study we use numerical models to investigate how minibasins subside in response to density-driven downbuilding. We show that minibasins subsiding in isolation result in simple symmetric minibasins with relatively simple internal stratigraphic patterns. In contrast, where minibasins form in closely spaced arrays and subside at different rates, minibasins can kinematically interact due to complex patterns of flow in the encasing salt, even during simple density-driven subsidence. More specifically, we show that minibasins can: 1) prevent nearby minibasins from subsiding; 2) induce lateral translation of nearby minibasins; and 3) induce tilting and asymmetric subsidence of nearby minibasins. We conclude that even in areas where no regional or dominant salt flow regime exists, minibasins can still be genetically related and that minibasin subsidence histories cannot be fully understood if considered in isolation.

Introduction

Minibasins are small basins formed by subsiding into relatively thick autochthonous or allochthonous salt (e.g. Jackson and Hudec, 2017). Due to the specific properties of salt, which can flow under very low stresses, subsidence rates of minibasins can be orders of magnitude higher than subsidence rates in crustal basins, reaching values of up to 10,000 m/myr (Worrall and Snelson, 1989). Because they can contain important thicknesses of sedimentary rocks that may include potential hydrocarbon reservoirs, minibasins have been widely studied in hydrocarbon-bearing salt basins (e.g. Hudec and Jackson, 2007).

32 The stratigraphic infill of minibasins provides a record of their subsidence histories. In simple
33 terms, minibasin stratal geometries reflect the interplay between the two primary controls; minibasin
34 subsidence and sediment accumulation. On the one hand, the bulk sediment accumulation rate is
35 constrained by the sediment delivery system. On the other hand, the subsidence rate of a minibasin, which
36 creates the accommodation space for new sediment, depends on minibasin geometry and density, and the
37 patterns and vigor of salt flow below and around the minibasin (e.g. Hudec et al. 2009). As a result of the
38 strong coupling between minibasin subsidence and sedimentation, changes in subsidence style are recorded
39 by synkinematic stratal packages within minibasins (e.g. Giles and Lawton, 2002; Prather, 2003; Giles and
40 Rowan, 2012; Sylvester et al., 2015).

41 Based on 2D seismic reflection data from the northern Gulf of Mexico, Rowan and Weimer (1998)
42 document different types of seismic-stratigraphic packages that can be linked to different styles of
43 minibasin subsidence. Bowl- or layer-shaped symmetric packages record a broadly symmetric subsidence,
44 while asymmetric subsidence and minibasin tilting result in wedge-shaped packages. In the simplest
45 possible geometry, a minibasin that has a purely vertical subsidence history would be characterized by
46 vertically stacked, symmetrical, bowl-shaped depocenters (Fig. 1A). Many other stratal geometries are
47 possible though. For example a basal symmetric ‘bowl’ overlain by an asymmetric ‘wedge’ indicates and
48 initially symmetric subsidence followed by minibasin tilting and subsequent asymmetric subsidence (Fig.
49 1B and C). Thus, minibasin depocenters do not necessarily stack vertically and need not be symmetrical,
50 as they may be wedge-shaped and shift gradually or abruptly (Fig. 1B and C). The transition from a bowl-
51 to a wedge-shaped package is interpreted by Rowan and Weimer (1998) as the timing of minibasin welding.
52 However, Hudec et al. (2009) propose other non-welding related processes that can also lead to asymmetric
53 subsidence, including the response to an asymmetric sediment load, syn-subsidence shortening and
54 horizontal translation during canopy spreading.

55 Minibasin subsidence is commonly studied by considering the minibasin as an isolated element.
56 Internal stratal geometries of isolated minibasins would passively record the interplay between the inflation
57 of surrounding salt structures as the minibasin subsides, and the sediment accumulation in the minibasin
58 (e.g. Koyi, 1998; halokinetic sequences, Giles and Lawton, 2002, Giles and Rowan, 2012). However,
59 minibasins are rarely found in isolation, and are instead part of arrays of closely spaced minibasins bounded
60 by complex networks of salt walls and diapirs forming minibasin provinces. Minibasin provinces form in
61 different types of tectonic settings, ranging from collision zones such as the Precaspian and Sivas to passive
62 margins such as the northern Gulf of Mexico and Brazil (e.g. Volozh et al., 2003; Callot et al., 2014 Worrall
63 and Snelson, 1998; Fiduk and Rowan, 2012; Rowan and Vendeville, 2006). During shortening of minibasin
64 provinces, contraction is preferably accommodated within the weaker salt and as a result, diapirs become

65 squeezed or welded shut (e.g. Rowan and Vendeville, 2006). During their translation minibasins can
66 interact with each other as they collide, jostle and/or slide past one another resulting in complex geometries
67 (e.g. Rowan and Vendeville, 2006; Callot et al., 2016; Duffy et al., 2017). However, minibasins may still
68 exhibit complex stratigraphic geometries indicative of complex subsidence histories in cases when
69 shortening was not coeval with subsidence and/or where minibasins have not collided or are not welded
70 laterally (e.g. Jackson et al., 2019). This is especially true in settings where adjacent minibasins can have
71 very variable subsidence rates and where apparently isolated minibasins can still be filled by sediments
72 (e.g. continental basin-fill areas *sensu* Banham and Mountney, 2013) (Fig. 2). One question that has not
73 been previously addressed is whether adjacent minibasins can influence each other and interact through salt
74 flow without colliding or being welded together.

75 In this work we study the interactions between adjacent minibasins separated by diapirs subsiding
76 into a homogenous salt layer with no regional tectonics (e.g. shortening) or dominant regional salt flow.
77 For this purpose we perform a numerical modeling study that consists of several numerical simulations
78 performed with a 2D finite-element code. The goal of this study is three-fold: first, to demonstrate that
79 within arrays of minibasins subsiding at different rates, minibasins can influence adjacent ones by
80 perturbing the salt flow around them; second, to observe and describe the different ways in which minibasin
81 interactions can occur; third, to describe how minibasin stratal patterns record kinematic interactions
82 between adjacent minibasin.

83 Numerical method and model setup

84 We use the 2D finite-element code MVEP2 (Thielmann and Kaus, 2012, Johnson et al., 2013).
85 MVEP2 solves the equations of conservation of mass and momentum for incompressible materials with
86 visco-elasto-plastic rheologies, and employs Matlab-based solvers MILAMIN (Dabrowski et al., 2008) for
87 efficiency. The code uses a Lagrangian approach, where material properties are tracked by randomly
88 distributed markers that are advected according to the velocity field that is calculated in a regular, non-
89 deformable, numerical grid. The method and numerical implementation is explained in detail in Kaus, 2010.

90 Two rock phases are used in the model: a phase corresponding to salt rock and one to sediments.
91 Salt is modelled as a linear viscous fluid with a viscosity of 10^{18} Pa s (e.g. Mukherjee et al., 2010) and a
92 density of 2200 kg/m^3 (i.e. halite). Sediments are modelled as visco-plastic materials, with a brittle rheology
93 that is characterized by their cohesion (C) and effective friction angle (Φ). In the simulations, the color of
94 the deposited sediments changes every 0.5 myrs for visualization purposes only (i.e. there is no change in
95 physical properties of the sediments associated with the color change).

96 Densities (ρ) of salt and sediment phases are modelled as constant and homogenous. Sediment
97 density (ρ_{sediment}) is set higher than salt density, so that sediment-filled minibasins sink due to excess density.
98 Although this is a major simplification for minibasin initiation (see Hudec et al., 2009), the approach allows
99 spontaneous density-driven subsidence of minibasins from the very beginning of the simulations.
100 Furthermore, this assumption may be valid where minibasin deposits may be dense enough for density-
101 driven subsidence to occur from the moment of deposition (e.g. evaporitic and/or aeolian settings;
102 Prochnow et al., 2006; Matthews et al., 2007; see Fernandez et al., 2017). Sediments do not compact in the
103 simulations presented here.

104 Sedimentation in the models is simulated by vertically displacing a reference level according to a
105 specified aggradation rate. For each time step, the model assumes that the depositing sediments fill the
106 space up to the horizontal reference level. Therefore, the thickness of each newly deposited layer in the
107 model will depend both on the imposed aggradation rate and the subsidence of the underlying minibasin,
108 the latter creating extra accommodation space (e.g. Fernandez and Kaus, 2015). Numerically, this process
109 is implemented by converting any particle of “air-phase” below the reference-level to “sediment-phase” at
110 each time step (Fig. 3). There is no erosion in the numerical simulations presented here.

111 Two geometric model setups were used: control simulations with a single seeded minibasin, and
112 simulations with non-seeded arrays of minibasins (Fig. 4). Both setups start with an initial 1000 m thick
113 flat layer of salt (Fig. 4). The modelling domain for simulations with non-seeded minibasin arrays is 30 km
114 wide by 4 km high (Fig. 4). The model dimensions are enough to allow the formation and evolution of
115 several km-scale minibasins and thus are appropriate to represent sub-domains of salt-tectonic systems
116 containing minibasin arrays. This setup does not contain a pre-kinematic sediment layer on top of the salt,
117 and thus minibasin position is not explicitly imposed during the simulations. Instead, minibasins develop
118 spontaneously by density-driven subsidence and density overturn as sediments are added during the
119 simulation (e.g. Fernandez and Kaus, 2015). The control simulations for a single seeded minibasin have a
120 simulation domain of 10 km wide by 4 km high (Fig.4). In these control simulations, an initial layer of
121 sediments is added on top of salt at the center of the model. The purpose of this pre-kinematic layer is to
122 help nucleate or seed a minibasin at the center of the modelling domain. The smaller model dimensions are
123 enough to allow the formation of a single minibasin. This isolated minibasin subsides into a thick layer of
124 salt unperturbed by any other minibasins. The goal of the two setups is to compare the behavior and
125 resulting stratal geometries of a single isolated minibasin to the behavior and geometries associated with
126 minibasins subsiding as part of minibasin arrays.

127 In the simulations, 384 Lagrangian markers (hereinafter referred to as markers) are used per
128 element to track the material properties, resulting in over 10 million markers in the modelled area. These

129 markers have been perturbed from their initial regular position by applying random noise. The top, and left-
130 and right-hand boundaries of the modelling domain have a free-slip boundary condition imposed, meaning
131 that movement at the boundary can only occur parallel to the boundary. The bottom boundary of the domain
132 has a no-slip boundary condition. An internal free-stress boundary is achieved by using the “sticky-air”
133 layer approach (Cramer et al., 2012). This approach consists of adding a layer of zero density and relatively
134 low viscosity (three orders of magnitude lower viscosity than salt phase) on top of the sediment. By adding
135 this layer, topography can develop at the interface between the “sticky-air” and sediments (Fig. 4).

136 Different sediment densities were used in the simulations with non-seeded minibasin arrays (Table
137 1). For each density, we performed a sensitivity study of sediment properties (C and Φ , Table 1). All the
138 simulations within each sensitivity study have the position of the markers perturbed by the same noise so
139 that their positions are initially exactly the same, thus any differences between models is exclusively due
140 to differences in the parameters used for the sediments. Cohesion and friction angle determine the effective
141 strength of the minibasins, resulting in relatively weak (i.e. low cohesion and friction angle) or relatively
142 strong (i.e. high cohesion and friction angle) minibasins. The effective strength of a minibasin affects its
143 overall subsidence history and thus the contained stratal pattern.

144 During the numerical simulations, the velocity field calculated for each time step is used to extract
145 the X and Z velocity components across the model domain. X and Z velocity components are then averaged
146 per model domain column (in Z dimension) for the salt and for the sediments separately. The results show
147 the variation of the mean X and Z velocity of salt and sediments across the model length (in X dimension).
148 Positive value of X component of velocity indicate a flow towards the right, whereas negative values,
149 indicate flow in the opposite direction. Positive values of Z component of velocity indicate an upward flow,
150 whereas negative values indicate downward directed flow.

151 [Modeling Results](#)

152 In this section we describe three different simulations to illustrate the evolution of minibasins
153 formed by density-driven subsidence in the models. Simulation 1 shows the evolution of one single isolated
154 minibasin that formed from a pre-kinematic seed. Simulations 2 and 3 are two examples where no pre-
155 kinematic seeds were used and where arrays of minibasins formed spontaneously across the model. The
156 specific physical parameters of the three simulations are given in Table 2.

157 [Isolated minibasin sinking into thick salt](#)

158 In simulation 1, an initial pre-kinematic layer of sediments was added in the setup. This layer is 1
159 km long and 200 m thick, with a thicker (400 m-thick) central segment (Figs. 4, 5A). As sediments are
160 denser than salt in the models, the pre-kinematic layer subsides into the salt as soon as the simulation starts.
161 Density-driven subsidence of the pre-kinematic layer creates accommodation, so sediment deposition is

162 concentrated above the seed, forming a minibasin that is thickest at the center (Fig. 5A). As the minibasin
163 becomes thicker and, thus, more difficult to deform in the center, bending of the flanks is limited to very
164 narrow areas closest to the salt (cf. halokinetic folds of Giles and Lawton, 2002, Giles and Rowan, 2012).
165 The minibasin is initially widening as it subsides, until it starts narrowing upwards (after time ~ 1.56 myrs,
166 Fig. 5A). Overall, the isolated minibasin of simulation 1 subsides symmetrically throughout its history, with
167 this being recorded by symmetric stratal geometries within the minibasin (Fig. 5A).

168 The mean X and Z velocity components of simulation 1 are shown in Fig. 5B. The X component
169 of the mean salt velocity shows a positive peak to the right side of the minibasin, and a negative peak to the
170 left side of the minibasin (Fig. 5B). The two mean salt velocity peaks of the X components are of equal
171 magnitude ($V_{X_{\max}} = -V_{X_{\min}}$) (Fig. 5B). Away from the minibasin, the mean X component salt velocity
172 decreases gradually towards zero. The Z component of the mean salt velocity has the highest negative value
173 below the center of the minibasin ($V_{Z_{\text{mean}}}$) and two positive and equal value mean-velocity peaks to either
174 side of the minibasin ($V_{Z_{\text{peak}}} = V_{Z_{\text{rpeak}}}$) (Fig. 5B, red). Away from the minibasin, the mean Z salt velocity
175 decreases rapidly towards zero (Fig. 5B) As the isolated minibasin continues to subside into thick salt and
176 becomes thicker, more salt is evacuated from below the minibasin, thus the magnitude of mean salt velocity
177 X peaks increase until the minibasin welds at the base (Fig. 5B). Overall, salt velocity components indicate
178 that salt is expelled from below the subsiding minibasin to both sides equally, feeding flanking diapirs that
179 rise at similar rates. The generalized plot of the mean salt velocities for an isolated minibasin subsiding into
180 thick salt is shown in Fig. 5C.

181 The velocity field within the sediments is simpler, with the predominant Z component of the
182 velocity illustrating the subsidence of the minibasin as a downward directed symmetric flow (Fig. 5B).
183 Interestingly, when the minibasin is thin and weak enough to be able to accommodate deformation, the
184 velocity in Z direction shows a maximum value in the center of the minibasin decreasing toward the flanks;
185 this suggests deformation by folding. As the minibasin becomes thicker and stronger, the Z velocity shows
186 a constant value across the width of the minibasin, indicating no internal deformation (i.e. folding). In both
187 cases, the plots are symmetric.

188 Minibasin arrays sinking into thick salt

189 Having investigated how a single isolated minibasin subsides in simulation 1, we now explore the
190 evolution of minibasin arrays in simulations 2 and 3 (Fig. 6). These two simulations differ only in the
191 properties used to model the sediments (C and Φ , Table 2). Minibasin initiation process and overall
192 minibasin evolution is similar in both simulations, so both models are described together. The simulations
193 start with a flat layer of salt without a capping pre-kinematic sediment layer (Fig. 4A). Once the simulation
194 begins, the first sediment layer deposited is very thin, and not completely uniform in thickness due to the

195 random noise used to perturb the position of the markers. This tiny variation in the thickness of the early
196 sediment load produces differential subsidence into the salt and the formation of individualized thin
197 minibasins (Fig. 6 A, B; time ~ 1.96 m.y.). It must be emphasized that the initial layers of sediments are thin
198 compared to subsequent ones, because at this early stage the subsidence into salt is minimal. As the
199 minibasins subside into the salt, accommodation for new sediments is created on top of them, and the
200 initially thin minibasins eventually evolve into thicker and wider minibasins (Fig. 6 A, B; time ~ 1.96 m.y.
201 and onwards). The minibasins formed in the two simulations are numbered 1-13 (Fig. 6). In each simulation
202 6 to 10 minibasins form ranging in width and thickness (Fig. 6). A striking characteristic of these
203 simulations is that minibasins initiate asynchronously. Initially, thin sediment pods are roughly regularly
204 spaced across the model, but a few of them start subsiding faster than others (e.g. minibasins 3, 7, 10 and
205 13; Fig. 6). As a result, at any given time, minibasins of different thicknesses are subsiding at different
206 rates. The minibasins that subside fastest weld to the base of salt before the slower-subsiding minibasins.
207 Once the first minibasins (e.g. minibasins 3, 7, 10 and 13) weld, other minibasins (e.g. minibasins 1, 4, 6,
208 11 and 12) subside more quickly (Fig. 6). The process of minibasin formation described above results in
209 varied stratigraphic patterns within the minibasins. While some minibasins are symmetric in cross section,
210 many others exhibit very asymmetric geometries because of their complex subsidence histories. Next, we
211 will look in more detail at minibasin stratigraphic geometries.

212 *Symmetric minibasins*

213 *Symmetric minibasins having continuous subsidence*

214 Minibasin 3 (Fig. 6A) is an example of a minibasin that records symmetric subsidence throughout
215 its evolution, resulting in symmetric sediment fill composed of a basal symmetric bowl and overlying layers
216 (Fig. 7A). Minibasin 3 is also one of the depocenters that undergoes initially rapid subsidence. Minibasin 3
217 initiates with a bowl-shaped geometry (e.g. Fig. 7A), indicating a higher rate of subsidence in the center.
218 Minibasin 3 welds to the base of salt at around time: ~ 2.96 m.y. and therefore cannot subside vertically
219 anymore (Fig. 6A). However, due to the fact that overall salt level is rising (by evacuation of salt from
220 beneath surrounding minibasins), accommodation is still generated above the now-welded minibasin 3
221 (post-weld layer, Fig. 7A). As accommodation is created only by aggradation at this stage, layers deposited
222 after welding are thinner than during the preceding phase of vertical subsidence into thick salt (Figs. 6A
223 and 7A, time ~ 3.96 m.y. and onwards). Furthermore, the minibasin narrows-upwards at this stage, which
224 indicates salt inflation, driven by continued subsidence of other minibasins in the array, is faster than
225 sediment aggradation (Fig. 7A).

226 Other minibasins also display symmetric geometries (6, 10, and 13; Figs. 6 and 7). Minibasins 10
227 and 13 in simulation 3 (Fig. 6B) are adjacent, thus, we examine their velocity profiles together (Fig. 8). At
228 an early stage (Fig. 8A), subsidence of minibasins 10 and 13 is clearly visible in the mean Z sediment

229 velocity plot (marked with “S” in Fig. 8A). The horizontal and vertical flow of salt around minibasins 10
230 and 13 is visible in the mean salt velocity plots as more complex variations in amplitude (Fig. 8A).
231 However, the mean salt velocity profiles of minibasins 10 and 13 are very similar to the velocity profile of
232 a single isolated minibasin (cf. Figs. 5 and 8). As minibasins 10 and 13 continue to subside, horizontal (X)
233 and vertical (Z) salt flow velocities increase until welding, when they decrease again (Fig. 8). Minibasins
234 10 and 13 initiate first in simulation 3, so they subside into a fairly unperturbed salt layer. Furthermore,
235 they are far enough from each other so that their velocity perturbations do not overlap or affect each other.

236 *Symmetric minibasins having discontinuous subsidence*

237 Minibasins 9 and 12 also initiate early in simulation 3, at which time they develop symmetrical
238 geometries formed in response to early symmetric subsidence into thick salt (Fig. 6B and 8B). Early
239 subsidence of minibasin 12 is observed in the velocity plot as a characteristic mean sediment Z velocity
240 signature defined as a small downwards undulation (marked “S” in Fig. 8B). However, as denoted by the
241 absence of the same characteristic velocity signal in Fig. 8C, at time ~3.46 m.y., minibasin 12 is not
242 subsiding. By time ~4.76 m.y., minibasin 12 is again subsiding as indicated by the strong downward
243 undulation in Z velocity plot (marked “S”, Fig. 8D). We interpret that subsidence of minibasin 12 was
244 interrupted by a short period of no subsidence (Fig. 8C) before resuming rapid subsidence later in the
245 simulation (Fig. 8D). Why should this be so? To begin, the mean salt velocity signal beneath the early-
246 formed minibasin 12 is small compared to nearby minibasins 11 and 13, which are subsiding more rapidly
247 during this early phase (Fig. 8B). Later, the strong velocity perturbation generated by rapid subsidence of
248 minibasin 11 extends across minibasin 12, completely overprinting the (X and Z) velocity signal of
249 minibasin 12 (Fig. 8C). The lateral and upward flow of salt from beneath minibasin 11 towards minibasin
250 12 prevents minibasin 12 from subsiding. Instead, minibasin 12 moves laterally (compare Fig. 8C and D).
251 Minibasin 12 resumes its subsidence when minibasin 11 approaches the base of salt, and the rate of
252 expulsion of salt from beneath it decreases (Fig. 8D). At that stage, minibasin 12 resumes its symmetric
253 subsidence into a relatively quiescent salt compartmentalized in between two welded minibasins. Velocity
254 profiles of minibasin 12 at this stage are similar to the profiles of single isolated minibasins (compare Fig.
255 5 and 8D). We conclude that subsidence of minibasins can inhibit subsidence of another minibasin.

256 *Asymmetric minibasins*

257 Abrupt shifts of depocenters, where minibasins transition from a symmetric basal bowl-shaped to
258 an asymmetric wedge-shaped geometry, have been observed in the Gulf of Mexico (Rowan and Weimer,
259 1998), Precaspian Basin (Jackson et al., 2019) and in other salt basins (e.g. Sivas Basin; Kergaravat et al.,
260 2016). The bowl-to-wedge transitions observed in some minibasins of the Gulf of Mexico had been
261 interpreted as being the result of minibasin welding and subsequent lateral collapse (Rowan and Weimer,

262 1998). However, other mechanisms (e.g., syn-subsidence shortening, salt emplacement on top of minibasin)
263 may trigger tilting prior to welding (e.g. Hudec, 2009; Jackson et al., 2019).

264 Our models show minibasin tilting both before and after welding. About half of the minibasins in
265 Fig. 6 are symmetric, but the others show significant degrees of asymmetry, as indicated by sediment fill
266 that thickens towards one side of the minibasin. Several of the minibasins in our models begin tilting prior
267 to welding (e.g., minibasins 4 and 11, Fig. 7C-D). Others show tilting only after welding, and still others
268 show tilting both before and after (sometimes in opposite directions; e.g. minibasin 4, Fig. 4D). In this
269 section we discuss the origin of minibasin tilting both before and after welding, along with controls on the
270 direction and timing of tilt.

271 [Minibasin tilting prior to basal welding](#)

272 Minibasins 11 and 4 initiate as bowl-shaped minibasins, recording a period of symmetric
273 subsidence (Fig. 7C-D). On top of the symmetric bowl sequences, wedge-shaped sequences form due to
274 tilting and asymmetric subsidence. This initial tilting occurs prior to welding, and in both cases the tilt is
275 away from the nearest actively subsiding minibasin (Fig. 7C-D).

276 Minibasin 11 initiates relatively early in the simulation, at a time when the minibasin immediately
277 to its left, minibasin 10, is already subsiding rapidly (Fig. 7C, 8A and B). On its right side, by contrast,
278 minibasin 12 is much thinner and has a slower subsidence, which eventually stops at a later stage (cf. Fig.
279 8B, C). Even further to the right, minibasin 13 is nearly welded by the time minibasin 11 starts its main
280 phase of subsidence, so minibasin 13 is not expelling much salt (Fig. 8C). Thus, during its main phase of
281 subsidence, salt flow around minibasin 11 is asymmetric, most heavily influenced by expulsion of salt from
282 beneath minibasin 10 (Fig. 8B-C). In fact, the mean salt velocity signal around minibasin 11 shows that the
283 peak of V_{x11max} (positive value), is more prominent than the low V_{x11min} (negative value) (Fig. 8B). As a
284 result of this asymmetric salt flow around it, minibasin 11 starts subsiding asymmetrically (mean sediment
285 velocity marked with “A” in Fig. 8C), tilting towards the direction in which the salt flow has been increased
286 (to the right). Once minibasin 10 is welded and the associated salt flow stops (Fig. 8C), minibasin 11
287 resumes a purely symmetric subsidence, recorded by a constant-thickness sedimentary layer deposited just
288 before welding ($t=3.96$ myrs, Fig. 7C).

289 Other minibasins showing pre-welding asymmetric subsidence (e.g., minibasin 5, Fig. 7D), can
290 also be explained by appealing to tilting away from the nearest actively subsiding minibasin. Thus, we
291 conclude that tilting before welding of a minibasin can be induced by nearby minibasin subsidence and the
292 resulting alteration of salt-flow patterns.

293 *Minibasin tilting after basal welding*

294 Tilting of minibasins also occurs in the simulations after basal welding. For example, the upper,
295 strongly wedge-shaped sequences of minibasins 4, 7, and 11 all form late, after the minibasins weld (e.g.
296 Fig. 6 and 7B to C). Focusing again on minibasin 11, this minibasin welds at its base after a complex history
297 of tilting followed by a late stage of symmetric subsidence (Figs. 7C and 8D). When minibasin 11 welds,
298 minibasin 10 to its left is already welded, but minibasin 12 to its right starts subsiding more rapidly (Fig.
299 8D). Accelerated symmetric subsidence of minibasin 12 is reflected in the strong and symmetric velocity
300 signal visible in the X velocity component of the mean salt velocity plot (Fig. 8D). Expulsion of salt from
301 below minibasin 12 into the diapir between minibasins 11 and 12 induces pivoting of minibasin 11 away
302 from the inflating salt structure (Fig. 8D).

303 From this we conclude that once minibasins (symmetric or asymmetric) weld at their base, their
304 subsequent evolution (tilting vs symmetrical aggradation) depends not only on whether there are nearby
305 actively subsiding minibasins that can induce salt inflation and subsequent tilting, but also on the minibasin
306 basal geometry. Minibasin geometry affects the potential for the minibasin to pivot around the weld contact
307 point (e.g. Callot et al., 2016). We suggest that broadly symmetric minibasins with a centered basal weld
308 contact point are potentially more stable and able to resist tilting even in the presence of nearby subsiding
309 minibasins (e.g. minibasin 10, Fig. 6B). In contrast, minibasin with an off-centered basal weld contact point
310 (asymmetric minibasins), will more easily pivot and tilt (e.g. minibasin 4 and 11, Fig. 6).

311 *Discussion*

312 *'Competition' for salt between minibasins subsiding at different rates*

313 In our single-minibasin numerical simulations, minibasins subside symmetrically (e.g., Fig. 5).
314 Tilting before welding only occurs in our simulations with multiple minibasins, suggesting that the presence
315 of multiple minibasins subsiding at different rates facilitates the formation of asymmetric minibasins. In
316 the numerical simulations presented here, minibasins subside at different rates. If minibasin subsidence is
317 purely density-driven, thicker and bigger minibasins subside faster and thus displace salt at higher rates
318 than smaller and thinner minibasins. The salt being expelled from below each subsiding minibasin moves
319 into the surrounding salt structures (typically diapirs; Fig. 8). If several minibasins are subsiding
320 simultaneously, a complex salt flow will result from the combination of all the individual velocity
321 perturbations. Bigger velocity perturbations induced by bigger minibasins will overprint the smaller
322 velocity perturbations of smaller minibasins. Overall, subsiding minibasins affect each other's subsidence
323 histories through the velocity perturbations they induce in the salt flowing around them. We thus propose
324 that minibasins, even if not in contact or connected by a roof, are kinematically interacting, so that

325 subsidence history of each minibasin cannot be understood without looking at the subsidence history of the
326 surrounding minibasins.

327 Minibasin interaction styles and implications

328 Based on observations from our numerical models, we propose that interactions between adjacent
329 minibasins that are not in contact with each other can occur. However, we also found that some minibasins
330 within the arrays do not interact with other minibasins. The simplest possible scenario for lack of minibasin
331 interactions is the case in which a minibasin forms in isolation and subsides vertically through its evolution
332 resulting in purely symmetrical stratigraphic geometries (e.g. simulation 1, Fig. 5). Minibasins rarely form
333 in complete isolation in nature and are invariably part of broader minibasin arrays. However, within
334 minibasin arrays, a minibasin can also subside without interacting with adjacent minibasins if there are no
335 minibasins sinking nearby (minibasins 3, 10, and 12; Fig. 6). There are two factors that can influence if
336 minibasins within the array will interact. The first factor to consider is the timing of minibasin subsidence.
337 Some of the symmetric minibasins observed in our simulations are the ones that subside early in the
338 simulations, when other minibasins have not yet formed, and so, are effectively subsiding in isolation (e.g.,
339 minibasins 3 and 10, Fig. 6). In this regard, observations from the Green Canyon area in the deep-water
340 Gulf of Mexico support this scenario, since one of the minibasins that subsided earlier (Miocene) into a
341 thick salt canopy displays simple symmetric geometries as compared to the later subsiding minibasins
342 (Pliocene) that were formed coevally in between other minibasins (Moore and Hinton, 2013). Some other
343 minibasins in our simulations subside later within minibasin arrays and yet, also display overall symmetric
344 geometries. Late-subsiding minibasins may do so, after adjacent minibasins have grounded and thus are not
345 expelling any salt. As a result, these late-subsiding minibasins sink into a relatively unperturbed salt in
346 between grounded minibasins, and can subside symmetrically developing symmetric stratigraphic
347 geometries. Effectively, these late-subsiding minibasins are also not being affected by any salt flow
348 perturbation induced by nearby subsiding minibasins. The second factor that can explain the lack of
349 interactions within arrays of minibasins is the spacing or distance between subsiding minibasins. A
350 minibasin subsiding within an array may be far enough from the closest actively subsiding minibasin so
351 that it is not affected by the associated salt flow perturbations.

352 Having outlined the scenarios in which minibasins may not interact with other minibasins of the
353 array, we next discuss the cases in which minibasins do interact. As pointed out before, adjacent subsiding
354 minibasins can interact if they are close enough to affect each other. In our simulations, we have observed
355 numerous styles of minibasin interactions. While some interactions result in asymmetric stratal geometries
356 of the minibasins, other interactions do not necessarily result in asymmetric geometries.

357 In our simulations, we have observed two interaction styles that do not necessarily result in
358 asymmetric geometries of the minibasins. First, actively subsiding thick minibasins can prevent other
359 nearby thinner minibasins from subsiding (e.g., minibasins 6 and 12; Fig. 9B). Once the actively subsiding
360 minibasins are grounded, the minibasin whose subsidence was prevented, can resume its symmetric
361 subsidence again (Fig. 9B). An important implication of discontinued subsidence is that minibasins can
362 have incomplete stratigraphic sections, with hiatuses representing the time when subsidence was not
363 occurring even if the depositional systems feeding them were still active (Fig. 9B and C). Second, actively
364 subsiding minibasins can induce the lateral translation of a thinner nearby minibasin (Fig. 9C, E). In fact,
365 many of the minibasins in the simulations of minibasin arrays display a certain amount of lateral translation
366 (indicated by the arrows in minibasins 4, 6, 11 and 12 of Fig. 6). Each arrow indicates the distance between
367 the initial and final position of the depocenter during the simulation. Translation occurs wherever there is
368 an asymmetry in horizontal flow on either side of a minibasin (e.g., minibasin 12 in Fig. 8). Thicker and
369 more massive minibasins are more difficult to translate, and we do not see translation in our models after
370 basal welding. As in the case of minibasins with discontinued subsidence, minibasins that are laterally
371 translated, may also have an incomplete stratigraphic sequence.

372 Another style of minibasin interaction is one that can lead to the formation of asymmetric
373 minibasins before basal welding occurs (Fig. 9D). If subsidence of nearby minibasins results in an
374 asymmetric salt flow around a minibasin, salt from below the minibasin is evacuated preferentially towards
375 one side. This scenario results in the tilting of the minibasin towards the side of preferential evacuation, as
376 recorded by thickening of the sedimentary sequence that is being deposited on top of the asymmetrically
377 subsiding minibasin. For example, minibasins 4 and 11 tilted before basal welding (Fig. 6, 7, 8). The
378 observation that minibasins can tilt before basal welding has important implications for interpreting weld
379 timing. The bowl-to-wedge transitions in the stratal geometries of minibasins has previously been linked to
380 the basal welding of minibasins (Rowan and Weimer, 1998). Our numerical models illustrate that this
381 interpretation may not be appropriate in all cases, as pre-welding tilting of minibasins can occur due to the
382 kinematic interactions between minibasins (see also Jackson et al., 2019).

383 Finally, as observed in our models, minibasin interactions can also induce tilting of a grounded
384 minibasin (Fig. 9F). Once a minibasin is grounded, the salt displaced by an adjacent subsiding minibasin
385 can cause the grounded minibasin to tilt away from the inflating salt structure (e.g. Minibasin 7; Fig. 6A).
386 After welding, subsidence of minibasin 8 to the right induced the tilting away of minibasin 7 to the left
387 (Fig. 6A). Tilting of asymmetric minibasins after welding is also common in the simulations. In some cases,
388 the tilt direction reverses after welding (e.g. minibasins 4 and 11, Fig. 6, 7 and 8), resulting in the stacking
389 of wedge-shape sequences that thicken in opposite directions.

390 Although our models have addressed the interactions between minibasins from a two-dimensional
391 perspective, salt flow is a very three-dimensional process. In contrast to our models, in a three-dimensional
392 framework, salt can be expelled in any direction within the salt volume, across salt walls and diapirs
393 surrounding the minibasins. On the one hand, because salt may spread in more directions, it is likely that
394 the interactions among nearby minibasins described here (e.g. discontinued subsidence and tilting) would
395 be mitigated. On the other hand, it means that there is more potential for differential salt flows in the
396 horizontal plane; this could cause minibasin rotation about a sub-vertical axis as observed in physical
397 models where minibasins collide (e.g. Rowan and Vendeville, 2006; Callot et al., 2016).

398 Conclusions

399 Two-dimensional numerical models were performed to study a scenario in which minibasins were
400 initiated and subsided into salt at different rates, without slope-driven regional salt flow or tectonic
401 deformation. The goal of the study was to test the hypothesis that minibasins are able to interact through
402 the complex patterns of salt flow that results when adjacent minibasins are subsiding at different rates (e.g.
403 Jackson et al., 2019). Our models show that minibasins do indeed interact, and that minibasins may tilt,
404 translate, or experience delays in subsidence due to subsidence of nearby minibasins. These interactions are
405 all results of a competition between subsiding minibasins for the finite available salt volume. Ultimately,
406 the complex subsidence history is reflected in the complex patterns of minibasin sedimentation.

407 Minibasin interpretation usually assumes either vertical density-driven subsidence, or subsidence
408 dominated by a regional salt flow. Regional salt flow can indeed be important, especially in areas where
409 large-scale basinward movement of salt has been identified or where the basin experiences regional
410 tectonics. However, minibasins do not necessary have undergone a simple history of purely vertical
411 subsidence in tectonically quieter areas. Locally induced perturbations to the salt flow can be caused by the
412 differential rates of salt expulsion related to the different subsidence rates of minibasins. The interactions
413 illustrated by the numerical models shown in this study suggest that minibasin subsidence occurs in a
414 dynamic system in which minibasins do not act as mere recorders of the salt flow around them, but rather
415 they are also the drivers that can influence and alter that salt flow by themselves.

416 We suggest that interactions between adjacent minibasins that have not collided should be
417 considered when interpreting stratal patterns within minibasins, particularly in areas where the salt-tectonic
418 processes are thought to be purely vertical. The models shown in this work illustrate that even in such areas,
419 minibasins can have complex subsidence histories due to interactions between them.

420 Acknowledgements

421 We thank Boris Kaus for developing and making available the numerical code MVEP2. We thank
422 Nancy Cottington for figure drafting. The project was funded by the Applied Geodynamics Laboratory
423 (AGL) Industrial Associates program, comprising the following companies: Anadarko, Aramco Services,
424 BHP Billiton, BP, CGG, Chevron, Condor, EcoPetrol, EMGS, ENI, ExxonMobil, Hess, Ion-GXT, Midland
425 Valley, Murphy, Nexen USA, Noble, Petrobras, Petronas, PGS, Repsol, Rockfield, Shell, Spectrum,
426 Equinor, Stone Energy, TGS, Total, WesternGeco, and Woodside
427 (<http://www.beg.utexas.edu/agl/sponsors>). The authors received additional support from the Jackson
428 School of Geosciences, The University of Texas at Austin.

429 References

- 430 Banham, S. G., and Mountney, N. P., 2013, Evolution of fluvial systems in salt-walled mini-basins: A
431 review and new insights: *Sedimentary Geology*, v. 296, p. 142-166.
- 432 Barde, J.-P., Chamberlain, P., Galavazi, M., Gralla, P., Harwijanto, J., Marsky, J., and van den Belt, F.,
433 2002, Sedimentation during halokinesis: Permo-Triassic reservoirs of the Saigak Field, Precaspian
434 Basin, Kazakhstan: *Petroleum Geoscience*, v. 8, no. 2, p. 177-187.
- 435 Barde, J.-P., Gralla, P., Harwijanto, J., and Marsky, J., 2002b, Exploration at the Eastern Edge of the
436 Precaspian Basin: Impact of Data Integration on Upper Permian and Triassic Prospectivity: *AAPG*
437 *Bulletin*, v. 86, no. 3, p. 399-415.
- 438 Callot, J.-P., Ribes, C., Kergaravat, C., Bonnel, C., Temiz, H., Poisson, A., Vrielynck, B., Salel, J.-F., and
439 Ringenbach, J.-C., 2014, Salt tectonics in the Sivas basin (Turkey): crossing salt walls and
440 minibasins: *Bulletin de la Societe Geologique de France*, v. 185, no. 1, p. 33-42.
- 441 Callot, J.-P., Salel, J.-F., Letouzey, J., Daniel, J.-M., and Ringenbach, J.-C., 2016, Three-dimensional
442 evolution of salt-controlled minibasins: Interactions, folding, and megaflap development: *AAPG*
443 *Bulletin*, v. 100, no. 9, p. 1419-1442.
- 444 Cramer, F., Schmeling, H., Golabek, G. J., Duretz, T., Orendt, R., Buitter, S. J. H., May, D. A., Kaus, B. J.
445 P., Gerya, T. V., and Tackley, P. J., 2012, A comparison of numerical surface topography
446 calculations in geodynamic modelling: an evaluation of the 'sticky air' method: *Geophysical*
447 *Journal International*, v. 189, no. 1, p. 38-54.
- 448 Dabrowski, M., Krotkiewski, M., and Schmid, D. W., 2008, MILAMIN: MATLAB-based finite element
449 method solver for large problems: *Geochemistry, Geophysics, Geosystems*, v. 9, no. 4, p. Q04030.
- 450 Duffy, O. B., Fernandez, N., Hudec, M. R., Jackson, M. P. A., Burg, G., Dooley, T. P., and Jackson, C. A.
451 L., 2017, Lateral mobility of minibasins during shortening: Insights from the SE Precaspian Basin,
452 Kazakhstan: *Journal of Structural Geology*, v. 97, p. 257-276.
- 453 Fernandez, N., Duffy, O. B., Hudec, M. R., Jackson, M. P. A., Burg, G., Jackson, C. A. L., and Dooley, T.
454 P., 2017, The origin of salt-encased sediment packages: Observations from the SE Precaspian Basin
455 (Kazakhstan): *Journal of Structural Geology*, v. 97, p. 237-256.
- 456 Fernandez, N., and Kaus, B. J. P., 2015, Pattern formation in 3-D numerical models of down-built diapirs
457 initiated by a Rayleigh–Taylor instability: *Geophysical Journal International*, v. 202, no. 2, p. 1253-
458 1270.
- 459 Fiduk, J. C., and Rowan, M. G., 2012, Analysis of folding and deformation within layered evaporites in
460 Blocks BM-S-8 & -9, Santos Basin, Brazil: Geological Society, London, Special Publications,
461 v. 363, no. 1, p. 471-487.
- 462 Giles, K. A., and Lawton, T. F., 2002, Halokinetic Sequence Stratigraphy Adjacent to the El Papalote
463 Diapir, Northeastern Mexico: *AAPG Bulletin*, v. 86, no. 5, p. 823-840.

- 464 Giles, K. A., and Rowan, M. G., 2012, Concepts in halokinetic-sequence deformation and stratigraphy:
465 Geological Society, London, Special Publications, v. 363, no. 1, p. 7-31.
- 466 Hudec, M. R., and Jackson, M. P. A., 2007, Terra infirma: Understanding salt tectonics: Earth-Science
467 Reviews, v. 82, no. 1-2, p. 1-28.
- 468 Hudec, M. R., Jackson, M. P. A., and Schultz-Ela, D. D., 2009, The paradox of minibasin subsidence into
469 salt: Clues to the evolution of crustal basins: Geological Society of America Bulletin, v. 121, no.
470 1-2, p. 201-221.
- 471 Jackson, M. P. A., and Hudec, M. R., 2017, Salt Tectonics: Principles and Practice, Cambridge, Cambridge
472 University Press.
- 473 Jackson, C. A. L., Duffy, O. B., Fernandez, N., Dooley, T., Hudec, M., Jackson, M., & Burg, G. (2019).
474 The Stratigraphic Record of Minibasin Subsidence. PREPRINT
- 475 Johnson, T. E., Brown, M., Kaus, B. J. P., and VanTongeren, J. A., 2013, Delamination and recycling of
476 Archaean crust caused by gravitational instabilities: Nature Geoscience, v. 7, p. 47.
- 477 Kaus, B. J. P., 2010, Factors that control the angle of shear bands in geodynamic numerical models of brittle
478 deformation: Tectonophysics, v. 484, no. 1-4, p. 36-47.
- 479 Kergaravat, C., Ribes, C., Legeay, E., Callot, J.-P., Kavak, K. S., and Ringenbach, J.-C., 2016, Minibasins
480 and salt canopy in foreland fold-and-thrust belts: The central Sivas Basin, Turkey: Tectonics, v. 35,
481 no. 6, p. 1342-1366.
- 482 Koyi, H., 1998, The shaping of salt diapirs: Journal of Structural Geology, v. 20, no. 4, p. 321-338.
- 483 Matthews, W. J., Hampson, G. J., Trudgill, B. D., and Underhill, J. R., 2007, Controls on fluvio-lacustrine
484 reservoir distribution and architecture in passive salt-diapir provinces: Insights from outcrop
485 analogs: AAPG Bulletin, v. 91, no. 10, p. 1367-1403.
- 486 Moore, V. and Hinton, D., 2013, Secondary basins and sediment pathways in Green Canyon, deepwater
487 Gulf of Mexico AAPG Search and Discovery Article, AAPG Annual Convention and Exhibition,
488 Pittsburgh, USA (2013)
- 489 Mukherjee, S., Talbot, C. J., and Koyi, H. A., 2010, Viscosity estimates of salt in the Hormuz and
490 Namakdan salt diapirs, Persian Gulf: Geological Magazine, v. 147, no. 04, p. 497-507.
- 491 Prather, B. E., 2003, Controls on reservoir distribution, architecture and stratigraphic trapping in slope
492 settings: Marine and Petroleum Geology, v. 20, no. 6, p. 529-545.
- 493 Prochnow, S. J., Atchley, S. C., Boucher, T. E., Nord, L. C., and Hudec, M. R., 2006, The influence of salt
494 withdrawal subsidence on palaeosol maturity and cyclic fluvial deposition in the Upper Triassic
495 Chinle Formation: Castle Valley, Utah: Sedimentology, v. 53, no. 6, p. 1319-1345.
- 496 Rowan, M. G., and Weimer, P., 1998, Salt-sediment interaction, northern Green Canyon and Ewing Bank
497 (offshore Louisiana), northern Gulf of Mexico: AAPG Bulletin, v. 82, no. 5B, p. 1055-1082.
- 498 Rowan, M. G., and Vendeville, B. C., 2006, Foldbelts with early salt withdrawal and diapirism: Physical
499 model and examples from the northern Gulf of Mexico and the Flinders Ranges, Australia: Marine
500 and Petroleum Geology, v. 23, no. 9-10, p. 871-891.
- 501 Schuster, D. C., 1995, Deformation of Allochthonous Salt and Evolution of Related Salt-Structural
502 Systems, Eastern Louisiana Gulf Coast Salt Tectonics: A Global Perspective, *in* Jackson, M. P.
503 A., Roberts, D. G., and Snelson, S., eds., Volume 65, American Association of Petroleum
504 Geologists.
- 505 Sylvester, Z., Cantelli, A., and Pirmez, C., 2015, Stratigraphic evolution of intraslope minibasins: Insights
506 from surface-based model Stratigraphic Evolution of Intraslope Minibasins: AAPG Bulletin, v.
507 99, no. 6, p. 1099-1129.
- 508 Thielmann, M., and Kaus, B. J. P., 2012, Shear heating induced lithospheric-scale localization: Does it
509 result in subduction?: Earth and Planetary Science Letters, v. 359-360, p. 1-13.
- 510 Volozh, Y., Talbot, C., and Ismail-Zadeh, A., 2003, Salt structures and hydrocarbons in the Pricaspian
511 basin: AAPG Bulletin, v. 87, no. 2, p. 313-334.
- 512 Worrall, D. M., and Snelson, S., 1989, Evolution of the northern Gulf of Mexico, with emphasis on
513 Cenozoic growth faulting and the role of salt: Evolution of the northern Gulf of Mexico, with
514 emphasis on Cenozoic growth faulting and the role of salt, v. A, p. 97-138.

515

Table 1. Description and range of values of the physical parameters used in the simulations

Symbol	Unit	Definition	Range of values
L_x, L_z	km	Initial dimensions of model in x and z	10 to 30, 4
n_x, n_z	-	Number of nodes in x and z	100 to 300, 100
H_{salt}	km	Initial thickness of salt	1
C	MPa	Cohesion of sediments	0.0 to 3.0
ϕ	$^\circ$	Friction angle of sediments	1 to 30
ρ_{sed}	kg/m^3	Density of sediments	2500 to 2650
ρ_{salt}	kg/m^3	Density of salt	2200
ρ_{air}	kg/m^3	Density of “sticky air”	0
μ_{sed}	Pa s	Viscosity of sediments	10^{25}
μ_{salt}	Pa s	Viscosity of salt	10^{18}
μ_{air}	Pa s	Viscosity of “sticky air”	10^{15}
S	cm/year	Sediment aggradation rate	0.001 to 0.01

516

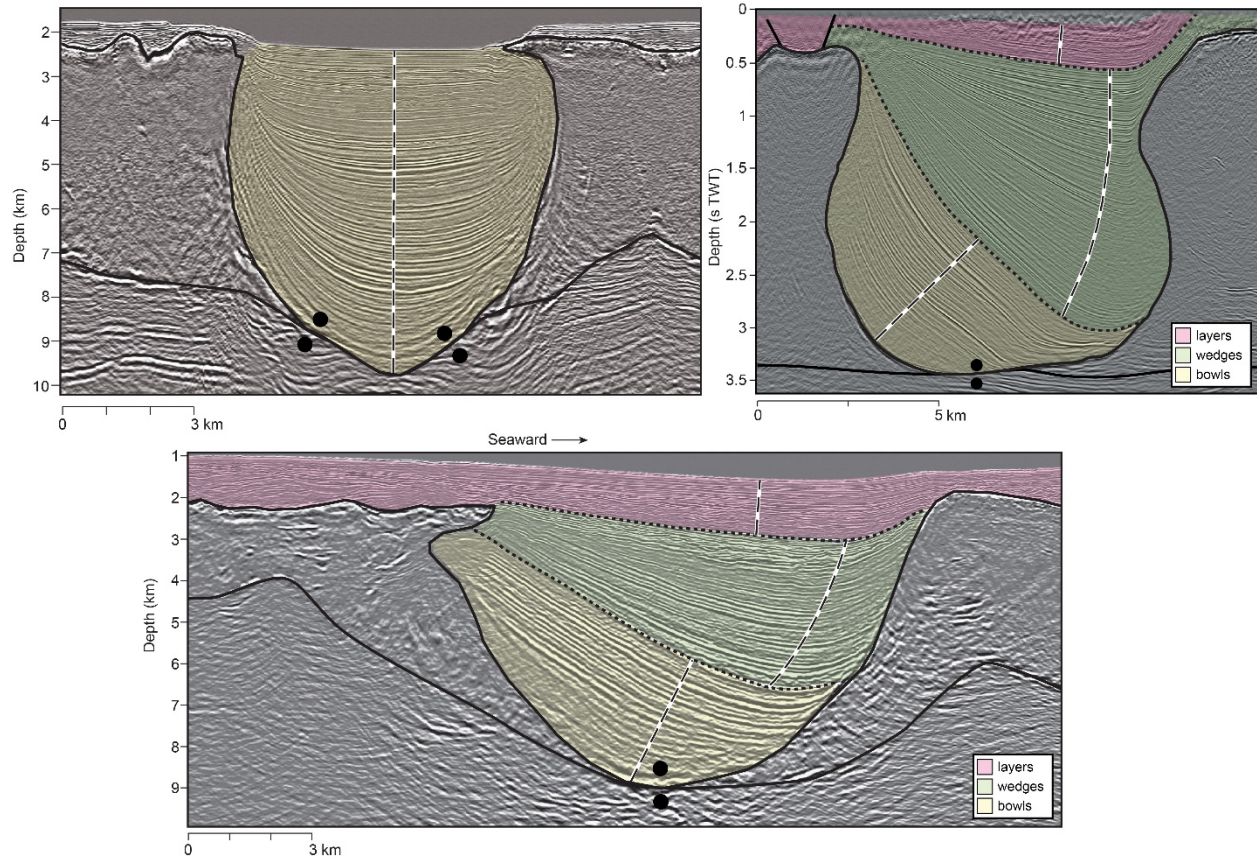
517

518

Table 2. Specific parameters used in the simulations described in the text.

	Simulation 1: Single Minibasin	Simulation 2: Minibasin Arrays	Simulation 3: Minibasin Arrays
L_x, L_z	10 km, 4 km	30 km, 4 km	30 km, 4 km
n_x, n_z	100, 100	300, 100	300, 100
C	0.0 MPa	0.0 MPa	0.2 MPa
ϕ	15°	15°	10°

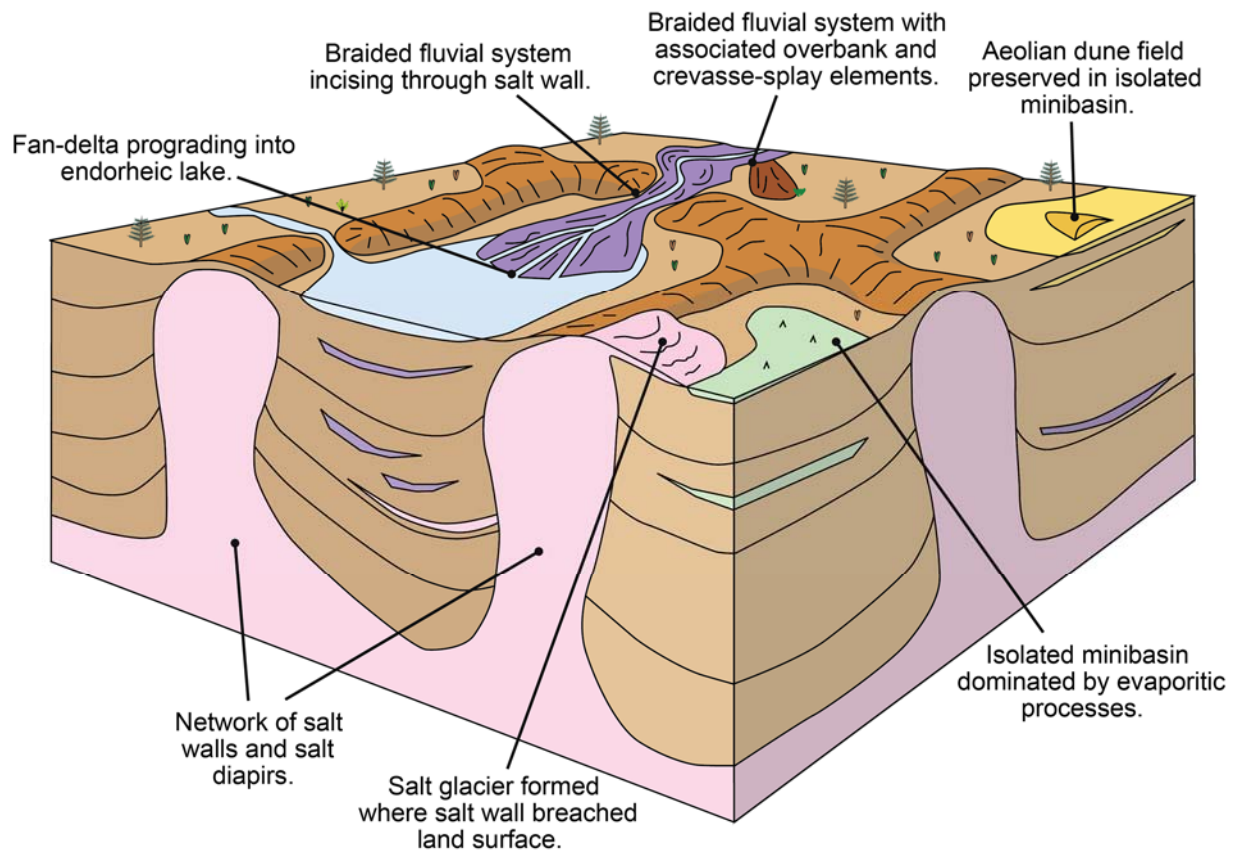
519



520

521 *Figure 1. Seismic examples of infill patterns of minibasins. Minibasins are located in the Gulf of Mexico (A and C, modified from*
 522 *Hudec et al., 2009) and in the Precaspian Basin (B, modified from Jackson et al., 2019). They illustrate the variable stratal*
 523 *geometries that can occur, from stacked depocenters resulting in symmetric minibasin (A) to abrupt shift of depocenters, as a*
 524 *result of a bowl- to- wedge (sensu Rowan and Weimer, 1998) transition resulting in asymmetric minibasins (B and C) .*

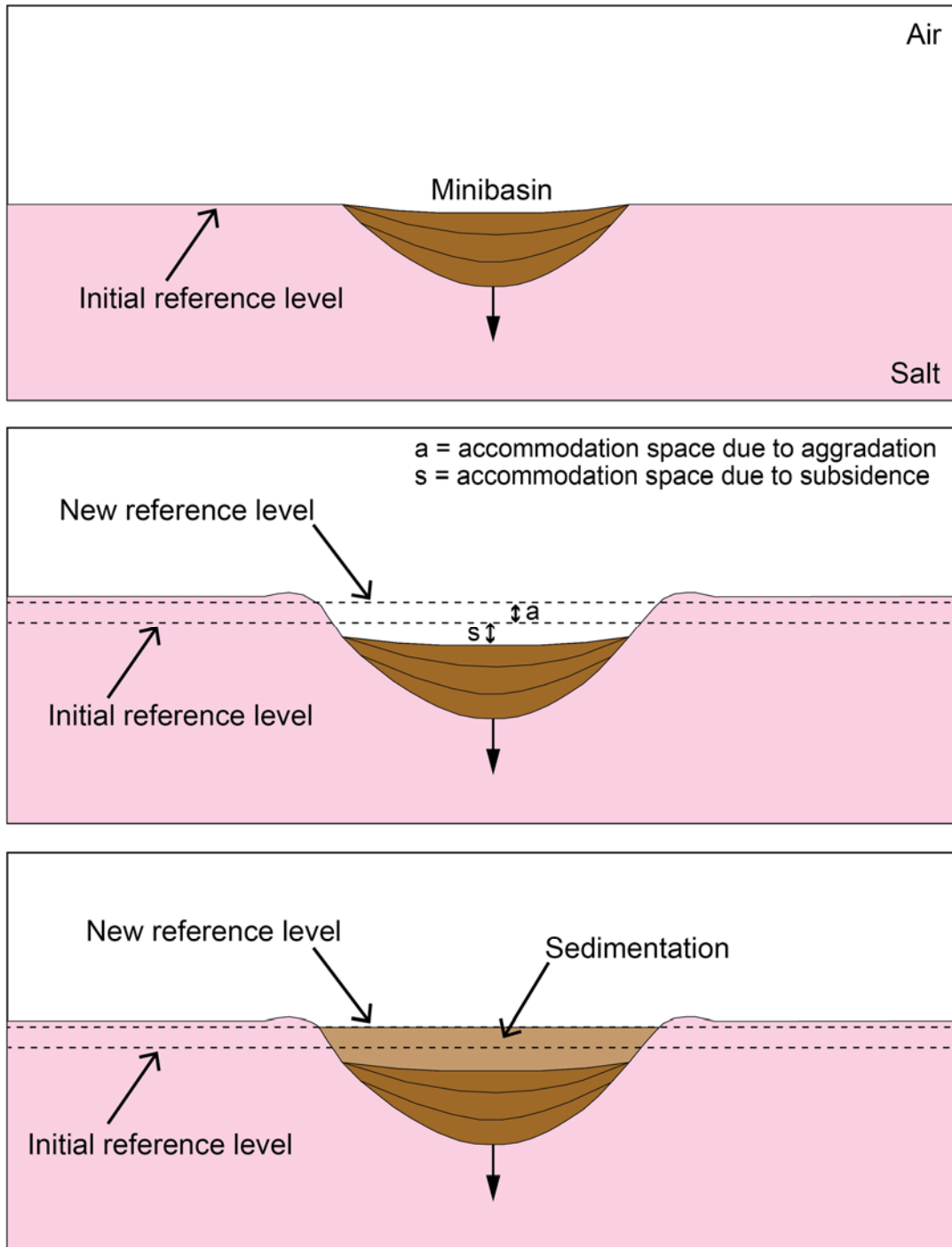
525



526

527 *Figure 2. The basin-fill model proposed by Banham and Moutney (2013) for areas such as the Precaspian Basin, predicts that*
 528 *adjacent and coeval minibasins can have very different subsidence rates. The model also predicts that minibasins that are*
 529 *isolated from the dominant sediment transport systems within the setting, can still be infilled by the deposits resulting from: a)*
 530 *evaporitic dominated processes and aelian dominated processes in the case of arid climates and b) lacustrine sediments in the*
 531 *case of more humid climates. (Modified after Barde et al. 2002).*

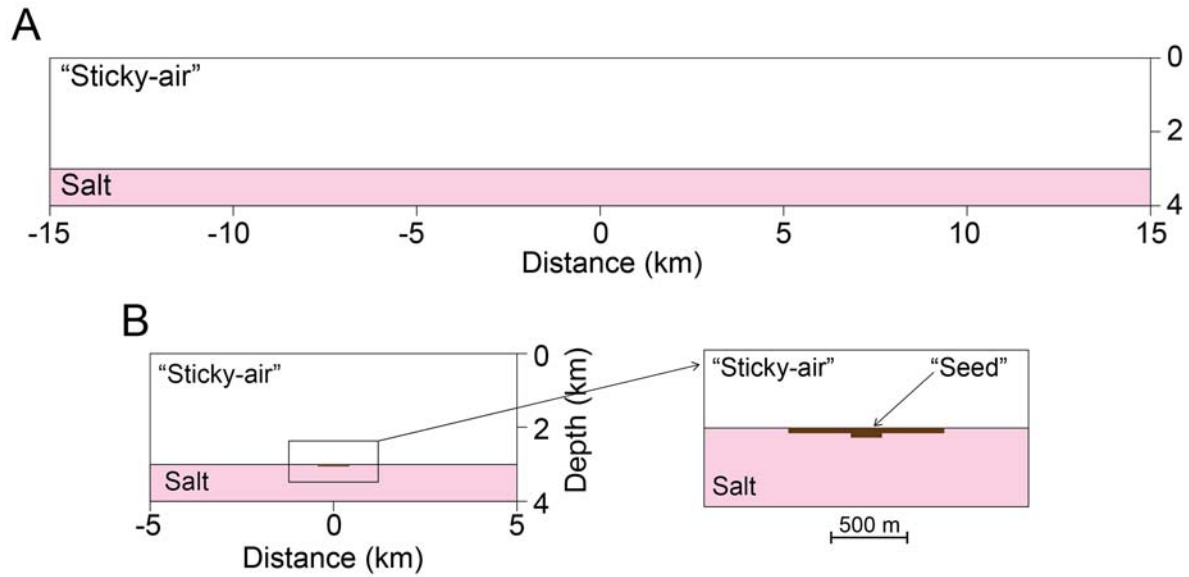
532



533

534 *Figure 3. Schematic sketch of the implementation of the sedimentation in the numerical code. The sedimentation algorithm, uses*
 535 *a horizontal flat reference level that aggrades vertically according to an imposed rate. As the minibasin subsides into salt, new*
 536 *accommodation space is created on top of the minibasin, both due to subsidence and due to aggradation. The newly created*
 537 *accommodation space is filled with sediments.*

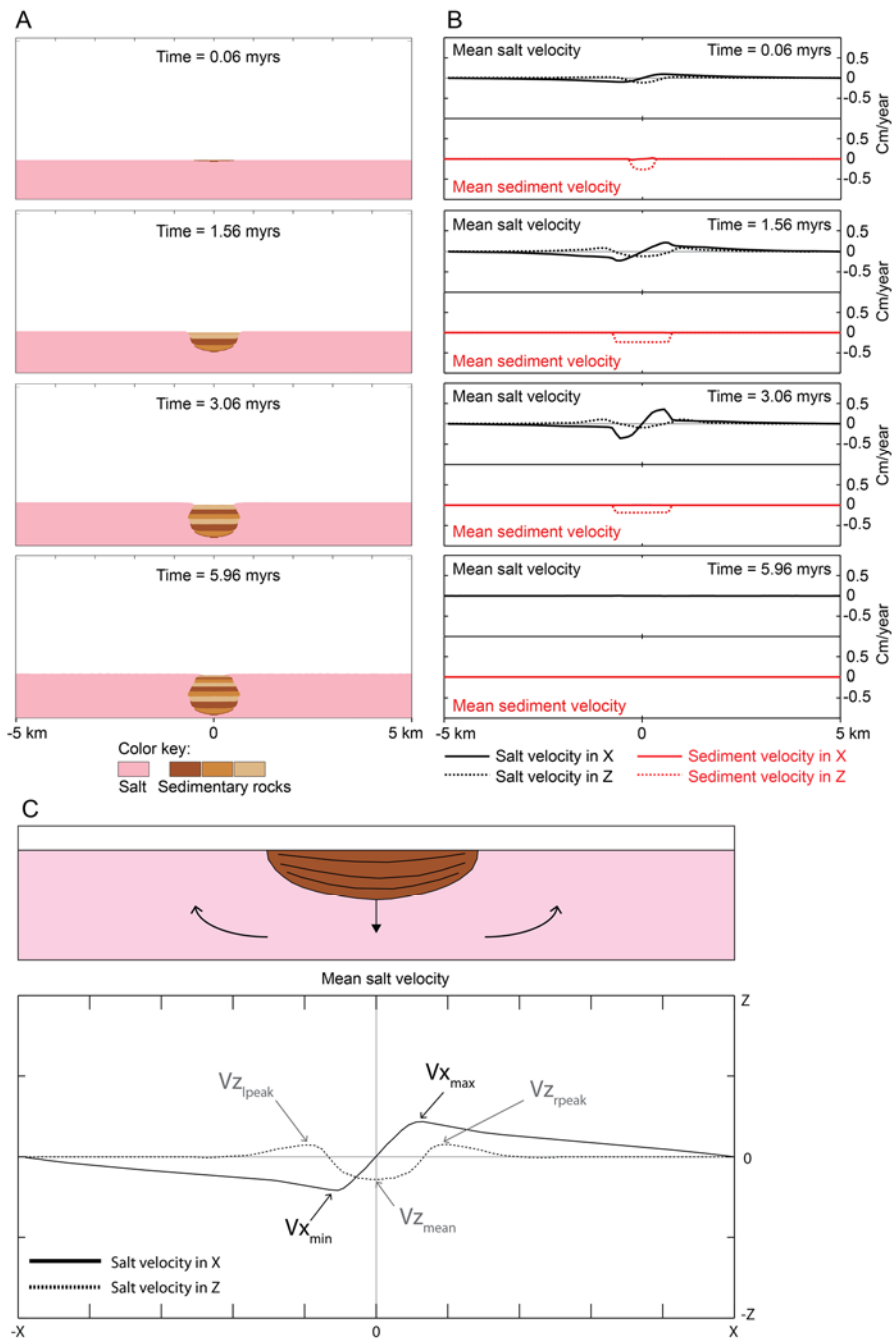
538



539

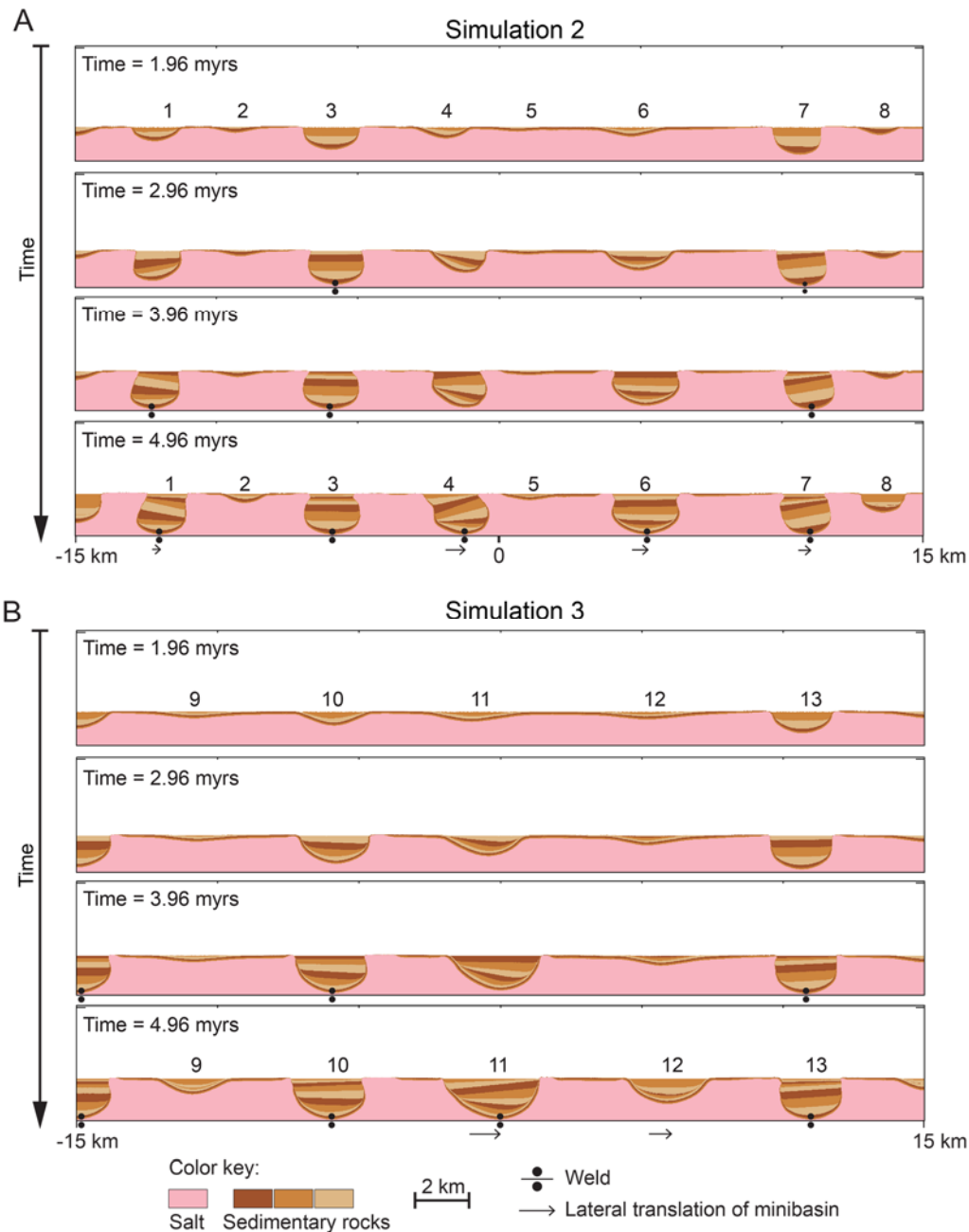
540 *Figure 4. A. Modeling domain setup for the two sets of simulations with minibasin arrays discussed throughout the text. There is*
 541 *no pre-kinematic sediment layer on top of the salt. Minibasin location is not explicitly imposed. Minibasins develop dynamically*
 542 *by density-driven overturn when sediments are added on top of the salt layer. B. Modelling setup used for control simulations.*
 543 *The control setup contains a pre-kinematic sediment layer that works as a "seed" that nucleates an isolated minibasin in the*
 544 *center of the domain. Control simulations are aimed at illustrating the geometries of an isolated minibasin subsiding into thick*
 545 *salt, without any other perturbation of the salt flow.*

546



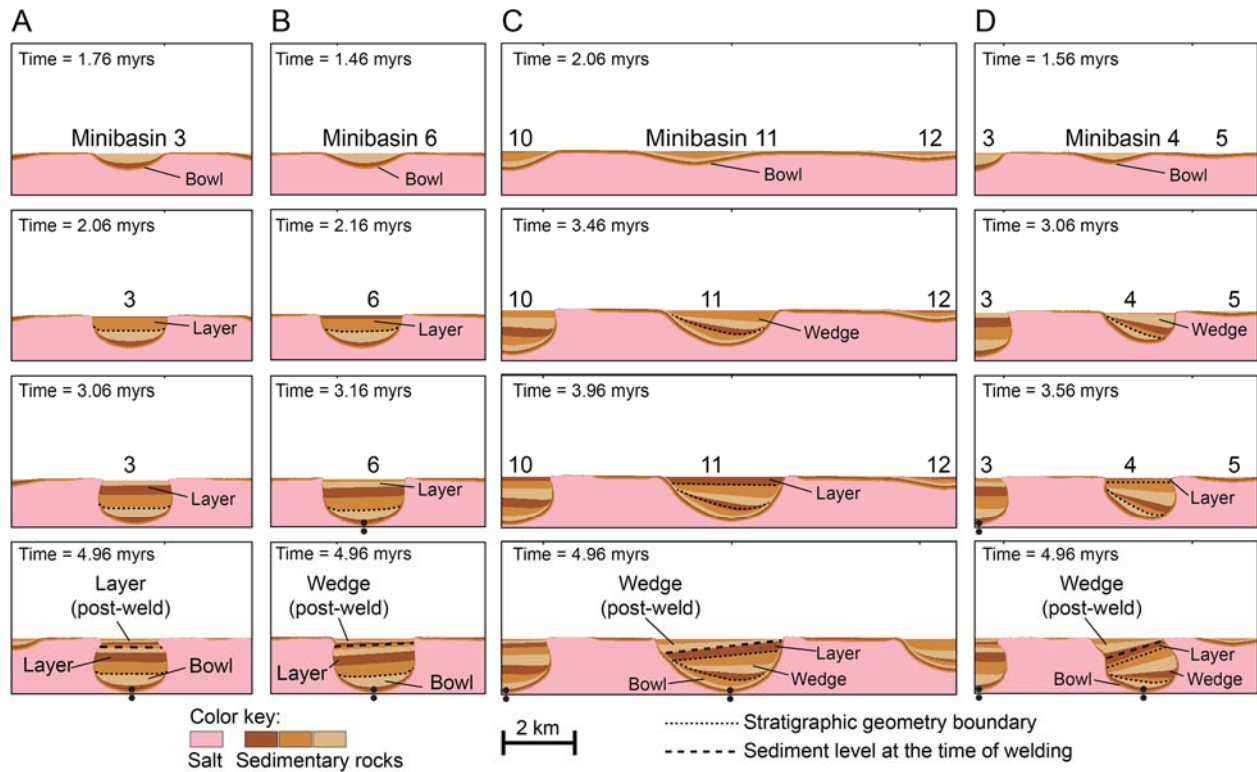
547

548 *Figure 5. A. Time evolution of simulation 1, which was performed with one seeded minibasin. In this simulation that serves as a*
 549 *control simulation, the imposed “seed” results in an isolated and model-domain-centered minibasin with symmetric stratal*
 550 *geometries. Sediment properties are $C = 0.0$ MPa, $\Phi = 30^\circ$ and $\rho_{sediment} = 2500$ kg/m³. B. Snapshots of the mean velocity values (X*
 551 *and Z components) within the salt (black line) and within the sediments (red line) for same time steps shown in A. C. Schematic*
 552 *plot of the mean velocity values within the salt expected for an isolated subsiding minibasin. The salt evacuated as the minibasin*
 553 *subsides is flowing symmetrically in both directions away from the minibasin, with the peak vertical flow occurring close to the*
 554 *minibasin.*



555

556 *Figure 6. Time evolution of two forward numerical simulations where no pre-kinematic seed was added. Simulations differ in the*
 557 *properties used to model the sediments. In simulation 2 (A), sediments are modelled with $C = 0.0$ MPa, $\Phi = 15^\circ$ and $\rho_{\text{sediment}} = 2500$*
 558 *kg/m³. In simulation 3 (B), sediments are modelled with $C = 0.2$ MPa, $\Phi = 10^\circ$ and $\rho_{\text{sediment}} = 2500$ kg/m³. Minibasins form and*
 559 *evolve by density driven subsidence in locations that have not been explicitly predefined. The resulting minibasins are numbered*
 560 *in the lowermost panel that represents the final time step (time = ~ 5 m.y.) and in a panel representing an intermediate time step*
 561 *(time = ~ 2 m.y.). One of the main characteristics of these two examples and other similar simulations is the different subsidence*
 562 *rates of the minibasins (minibasins can be initiated at different times) and the resulting complex stratal geometries of the*
 563 *minibasins, including symmetric (e.g. minibasins 3 and 6) and asymmetric geometries (e.g. minibasins 4 and 11).*

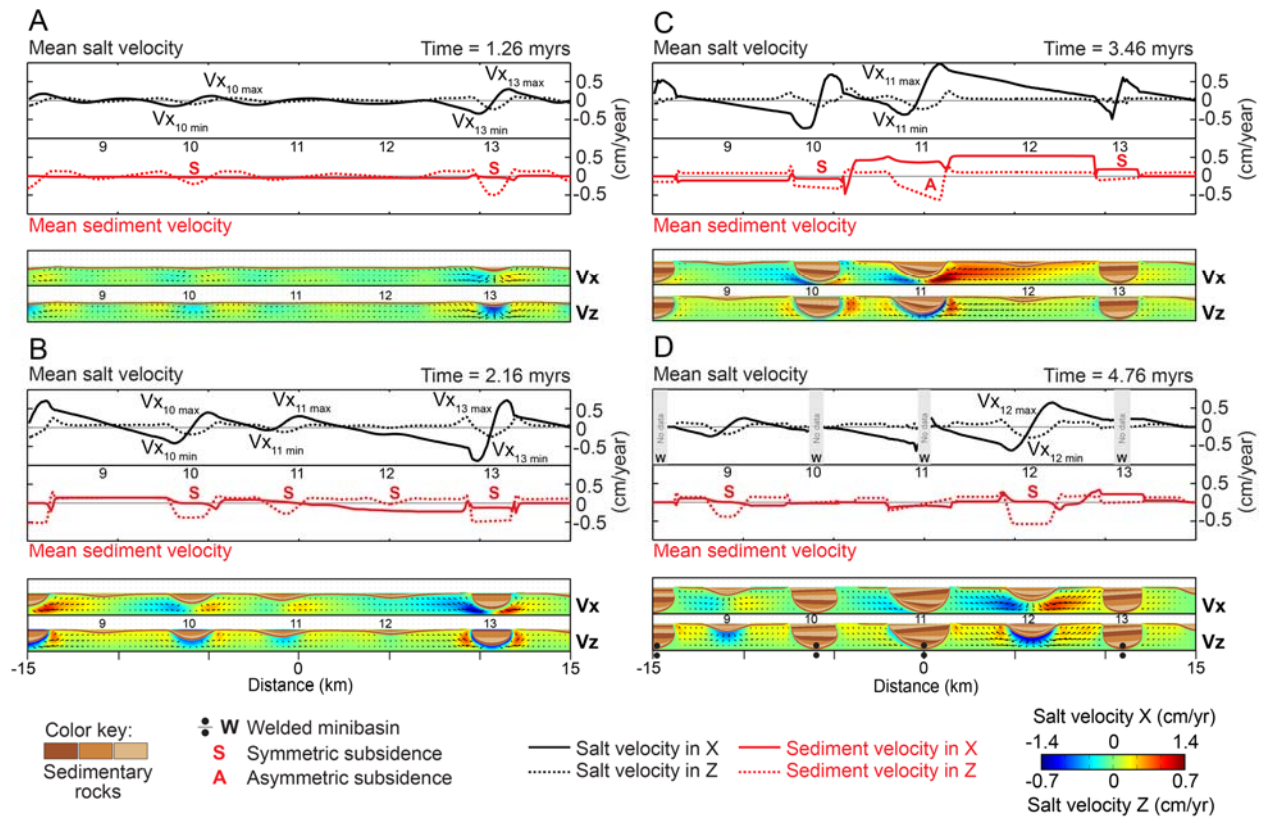


564

565 *Figure 7. Time evolution of several of the minibasins formed in simulations 2 and 3. Different minibasin geometries, symmetric or*
 566 *asymmetric, can be observed in the simulations. Minibasins 3 and 6 are overall symmetric minibasins (A and B), whereas*
 567 *minibasins 11 and 4 are strongly asymmetric minibasins (C and D). The dashed lines within the minibasins, indicate a change in*
 568 *the stratal geometries (bowl, wedge, layers sensu Weimer and Rowan, 1998) within the minibasins. Dashed thicker black line,*
 569 *indicates the approximate sediment infill level at the time of basal welding of the minibasin. These changes in geometry, correspond*
 570 *with changes in the subsidence style of the minibasins that as described in the text can be linked in some cases to minibasin*
 571 *interactions.*

572

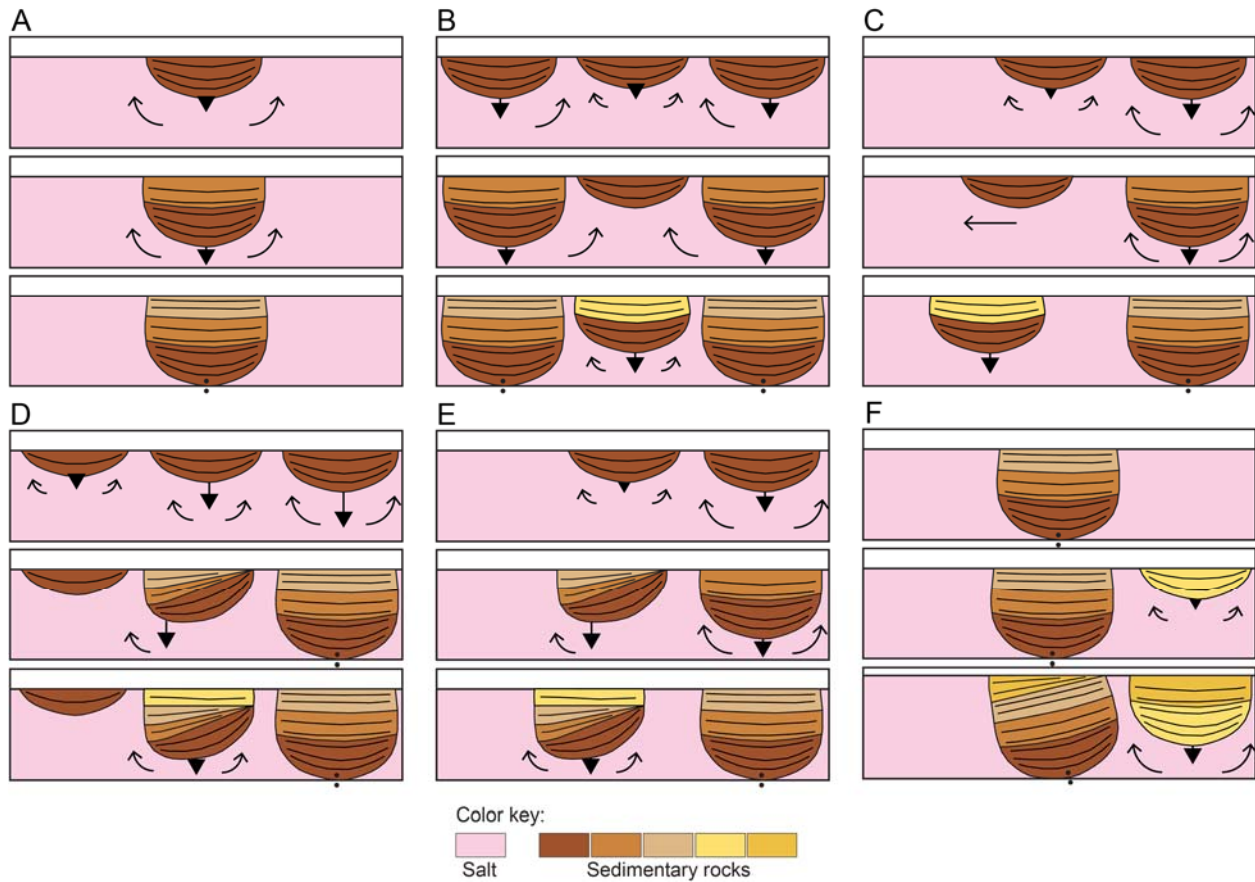
573



574

575 *Figure 8. A through D, snapshots of the evolution of simulation 3. Each time step is illustrated with four panels. Upper two*
 576 *panels contain the plots of the mean velocities (X and Z components) within the salt (black line, excluding the sediments) and*
 577 *within the sediments (red line, excluding salt). Lower two panels show the corresponding simulation output, with the sediments*
 578 *colored by the rock phase, and the salt colored by the value of the velocity component (X component for the upper panel, Z*
 579 *component for the lower panel) and velocity vectors.*

580



581

582 *Figure 9. Conceptual sketches of the minibasin interactions observed in the numerical simulations. A. Sketch of a simple scenario*
 583 *in which an isolated minibasin is subsiding vertically. B and C, sketches in which the effect of perturbations in the salt flow induced*
 584 *by adjacent minibasins may lead to preventing one minibasin from subsiding and/or translate it laterally. D, E, F. Sketches*
 585 *illustrating examples of potential interactions between minibasins that would result in differential subsidence histories and*
 586 *asymmetric stratal geometries.*

587